Supplemental material to this article can be found at:
http://dmd.aspetjournals.org/content/suppl/2020/07/26/dmd.120.000083.DC1

1521-009X/48/10/1092–1103$35.00
DRUG METABOLISM AND DISPOSITION
https://doi.org/10.1124/dmd.120.000083
Drug Metab Dispos 48:1092–1103, October 2020

Special Section on Natural Products: Experimental Approaches to Elucidate Disposition Mechanisms and Predict Pharmacokinetic Drug Interactions

Multiomics Profiling Reveals Protective Function of *Schisandra* Lignans against Acetaminophen-Induced Hepatotoxicity[S]

Caixia Yan,[1] Huimin Guo,[1] Qingqing Ding,[1] Yuhao Shao, Dian Kang, Tengjie Yu, Changjian Li, Haoran Huang, Yisha Du, He Wang, Kangrui Hu, Lin Xie, Guangji Wang, and Yan Liang

Key Laboratory of Drug Metabolism & Pharmacokinetics, State Key Laboratory of Natural Medicines, China Pharmaceutical University, Nanjing, P.R. China (C.Y., H.G., Y.S., D.K., T.Y., C.L., H.H., Y.D., H.W., K.H., L.X., G.W., Y.L.) and Department of Geriatric Oncology, First Affiliated Hospital of Nanjing Medical University (Jiangsu People's Hospital), Nanjing, P.R. China (Q.D.)

Received April 22, 2020; accepted June 30, 2020

ABSTRACT

The action principles of traditional Chinese medicines (TCMs) feature multiactive components, multitarget sites, and weak combination with action targets. In the present study, we performed an integrated analysis of metabonomics, proteomics, and lipidomics to establish a scientific research system on the underlying mechanism of TCMs, and *Schisandra* lignan extract (SLE) was selected as a model TCM. In metabonomics, several metabolic pathways were found to mediate the liver injury induced by acetaminophen (APAP), and SLE could regulate the disorder of lipid metabolism. The proteomic study further proved that the hepatoprotective effect of SLE was closely related to the regulation of lipid metabolism. Indeed, the results of lipidomics demonstrated that SLE dosing has an obvious callback effect on APAP-induced lipidic profile shift. The contents of 25 diglycerides (DAGs) and 21 triglycerides (TAGs) were enhanced significantly by APAP-induced liver injury, which could further induce liver injury and inflammatory response by upregulating protein kinase C (PKCβ, PKCγ, PKCδ, and PKCθ). The upregulated lipids and PKCs could be reversed to the normal level by SLE dosing. More importantly, phosphatidic acid phosphatase, fatty acid transport protein 5, and diacylglycerol acyltransferase 2 were proved to be positively associated with the regulation of DAGs and TAGs.

SIGNIFICANCE STATEMENT

Integrated multiomics was first used to reveal the mechanism of APAP-induced acute liver failure (ALF) and the hepatoprotective role of SLE. The results showed that the ALF caused by APAP was closely related to lipid regulation and that SLE dosing could exert a hepatoprotective role by reducing intrahepatic diglyceride and triglyceride levels. Our research can not only promote the application of multicomponent technology in the study of the mechanism of traditional Chinese medicines but also provide an effective approach for the prevention and treatment of ALF.

Introduction

TCMs are essential parts of the health care system for diagnosis, prevention, and treatment of diseases in several Asian countries and are considered a complementary or alternative medical system in many Western countries (Yan et al., 2018). However, the modernization and internationalization of TCM are always hampered by its chemical complexity, unknown targets, and combinatorial use tradition guided by esoteric principles (Zhang et al., 2019). Recent years saw many studies use "omics" technology to elucidate the biologic foundation of TCMs. For instance, proteomics has been revolutionized by Mass spectrometry (MS)-based methods and is frequently used to measure the therapeutic effect of TCM treatments (Ohyama et al., 2015; Selevsek et al., 2015; Lin et al., 2012; Lan et al., 2018; Liu et al., 2018; Zhang et al., 2018b). Metabonomics, another omics approach, can also provide a powerful

This study was supported by the Nature Science Foundation of Jiangsu Province [Grant BK20171395]; the National Nature Science Foundation of China [Grant 81530098]; and "Double First-Class" University project [Grant CPU2018GF01].

[1]C.Y., H.G., and Q.D. contributed equally to this work.

None of the authors have any financial conflicts of interest.

https://doi.org/10.1124/dmd.120.000083.

[S]This article has supplemental material available at dmd.aspetjournals.org.

ABBREVIATIONS: ACC1, acetyl CoA carboxylase 1; ALF, acute liver failure; ALT, alanine aminotransferase; APAP, acetaminophen; AST, aspartate aminotransferase; DAG, diglyceride; DGAT2, diacylglycerol acyltransferase 2; DGAT2i, inhibitor of DGAT2; FABP, fatty acid–binding protein; FASN, fatty acid synthetase; FATP, fatty acid transport protein; IS, internal standard; KEGG, Kyoto Encyclopedia of Genes and Genomes; L-FABP, liver-type fatty acid–binding protein; LPC, lysophosphatidylcholine; LPE, lysophosphatidylethanolamine; MPB, mobile phase B; NAC, *N*-acetylcysteine; OPLS-DA, orthogonal partial least squares–discriminate analysis; PA, phosphatidic acid; PC, phosphatidylcholine; PCA, principal component analysis; PE, phosphatidylethanolamine; PKC, protein kinase C; PNL, propranolol; PS, phosphatidylserine; SLE, *Schisandra* lignan extract; TAG, triacylglycerol; TCM, traditional Chinese medicine MS Mass spectrometry; GC-MS Gas chromatography-mass spectrometer; m/z mass-to-charge ratio; LC Liquid chromatography.

technique for the identification of noninvasive biomarkers and can improve the diagnosis of complex diseases (Emwas et al., 2015). So far, metabonomics has gained enormous attention in the TCM research because the elucidation of the metabolic pattern for different syndromes is the root for understanding the actions of TCMs (Li et al., 2013). In addition, fatty acids are important signal molecules that regulate many cellular processes, from inflammation to neural function. Altered lipid profiles associated with disease progression will provide new insights into the pathogenic mechanisms of chemically induced toxic activity in disease (Yang et al., 2016; Titz et al., 2018; Xu et al., 2019b). In a word, omics technologies provide an opportunity to understand the flow of information that underlies TCMs.

APAP overdose is the most common cause of acute liver failure (ALF), and even death, in the Western world (Bernal et al., 2015). Despite mechanisms of drug-induced liver injury having been extensively investigated to develop novel therapeutic strategies, current treatment options after APAP overdose are extremely limited (Bhushan and Apte, 2019). The main reason is that most of the patients seek medical attention late, when the injury is already formed and difficult to reverse. To date, *N*-acetylcysteine (NAC) is still the only clinically recognized pharmacological intervention in patients with APAP overdose. However, NAC intervention is only effective within 24 hours after APAP overdose. Long-term use of NAC is even harmful to recovery after APAP overdose (Athuraliya and Jones, 2009). Rational, effective approaches for the prevention and treatment of APAP-induced ALF are, therefore, urgently required. *Schisandra chinensis* (Turcz.) Baill, a Magnoliaceae family plant abundant in the East, is regarded as a medical herb in both TCM and Western herbal medicine (Panossian and Wikman, 2008). Many studies have shown that *Schisandra* lignans have various pharmacological effects, such as liver protection, antioxidation, anti–lipid peroxidation, anticancer, and anti–human immunodeficiency virus effects, and so on (Kuo et al., 2001; Panossian and Wikman, 2008; Li et al., 2014; Jiang et al., 2015; Zhang et al., 2020). In our previous study, a series of solvents (10%, 50%, and 90% of ethanol) were used to extract lignans, and the corresponding SLEs were defined as 10% SLE, 50% SLE, and 90% SLE. The hepatoprotective effect of SLEs on APAP-induced liver injury were compared via histopathological analysis and by determining the levels of alanine aminotransferase (ALT), aspartate aminotransferase (AST), glutathione, and superoxide dismutase in mice and primary hepatocytes, and NAC was used as a positive drug. The results demonstrated that SLE pretreatment could remarkably ameliorate APAP-induced ALF by reducing ALT, AST, and oxidative stress levels. The hepatoprotective activity of 50% SLE was significantly higher than that of 10% SLE and 90% SLE (Kang et al., 2019).

To date, the research on the hepatoprotective effect of *Schisandra* lignans was mainly focused on their apparent efficacy. To our knowledge, the integrated application of multiomics to characterize the APAP-induced hepatotoxicity and hepatoprotective effect of SLE has not yet been reported. The present study aimed to develop a practical strategy for identifying the targets and mechanism of the multicomponent action of TCMs and provide an effective approach for the prevention and treatment of ALF induced by APAP overdose. Based on the systematic biologic approaches of metabonomics and proteomics, it was proved that the APAP-induced hepatotoxicity and the hepatoprotective effect of SLE were positively correlated with the regulation of lipid metabolism. Then, the lipidomics approach was used to identify the lipids that mediate the SLE's hepatoprotective effect. APAP-induced hepatic toxicity was proved to enhance the levels of intrahepatic diglycerides (DAGs) and triacylglycerols (TAGs), which could be reversed to the normal level by SLE dosing.

Materials and Methods

Materials

Schisandra sphenanthera was purchased from Anhui Songshan Tang Chinese medicine, Ltd. (Bozhou, Anhui, China). APAP was purchased from Maclin Biochemical Co., Ltd. (Shanghai, China). Collagenase I, Percoll, 1,2-$^{13}C_2$-mycolic acid, methoxyamine hydrochloride, *N*-methyl-n-trimethylsilane trifluoroacetamide, phenylmethylsulfonyl fluoride, dithiothreitol, iodoacetamide, hexadecane diacylglycerol (C16:0), PF-06424439, lysophosphatidylcholine (LPC, 17:0), lysophosphatidylethanolamine (LPE, 14:0), phosphatidylcholine (PC, 14:0/14:0), phosphatidylethanolamine (PE, 14:0/14:0), TAG (17:0/17:0/17:0), and phosphatidylserine (14:0/14:0) were purchased from Sigma-Aldrich Chemicals (St. Louis, MO). 5-^{13}C-Glutamine was purchased from Cambridge Isotope Laboratories, Inc. (Tewksbury, MA). The assay kits for the measurement of ALT and AST were purchased from Nanjing Jiancheng Institute of Bioengineering (Nanjing, Jiangsu, China). High Performance Liquid Chromatography-grade acetonitrile and methanol were purchased from Merck (Merck Company, Darmstadt, Germany). Ultrapure-grade water was prepared by the Milli-Q system (Millipore Corporation, Billerica, MA).

Animals and Treatments

Animals. Male C57BL/6J mice (6 weeks, weighing 18–20 g) were purchased from Vital River Laboratory Animal Technology Co., Ltd. (Beijing, China) and housed under controlled conditions (25°C, 55%–60% humidity, and a 12-hour light/dark cycle) with free access to laboratory food and water. Animal welfare and all studies were strictly in compliance with animal care laws and guidelines and approved by the Animal Care and Use Committee of China Pharmaceutical University.

Preparation of SLE and APAP-Induced Liver Injury Model Mice. To prepare the SLE, *S. sphenanthera* was powdered, followed by filtration through a fine sieve (270 μm). The filtered powder was heated to reflux twice for 2 hours with 50% ethanol (w/w 1:10), and the supernatants were concentrated with rotary evaporator. *Schisandra* lignans were further extracted by 5× volume of ethyl acetate. The contents of Schisandrol A, Schisandrol B, Schisantherin A, Schisandrin A, and Schisandrin B were determined to control the quality of SLE, and the results are shown in Supplemental Table 1. After drying the solvent, SLE powder was dissolved with 20% PEG-400 solution to form SLE emulsion. To prepare APAP-induced liver injury model mice, APAP was dissolved in saline (0.9% NaCl), slightly heated, and injected intraperitoneally at a dosage of 400 mg/kg into mice. Then, the mice regained free access to water. A total of 21 mice were divided into three groups ($n = 7$). In the control group, the mice were only treated with blank solvent. In the APAP group, the mice were intraperitoneally administrated with APAP at a dose of 400 mg/kg. In the SLE + APAP group, SLE was administered intragastrically at a dosage of 500 mg/kg for three consecutive days (twice a day). In the propranolol (PNL) group and the PNL + APAP group, the mice were intraperitoneally administrated with PNL once at a dose of 80 mg/kg. Then, the mice were intraperitoneally administrated 400 mg/kg of APAP 1 hour after the last administration of SLE or PNL. All mice were sacrificed under anesthesia at 4 hours after intraperitoneal injection of APAP, and blood samples and liver tissues were collected on an ice plate.

Culture of Primary Mouse Hepatocytes

Primary mouse hepatocytes were cultured in accordance with our previously developed methods (Kang et al., 2019). The ethylene glycol tetraacetic acid solution (0.5 mM) was prepared in HEPES-buffered Hank's balanced salt solution (pH 7.4). The mouse liver was perfused with ethylene glycol tetraacetic acid solution for 5 minutes at 40°C. The portal vein of the liver was cut off rapidly, and the blood and calcium ions were removed. Then, the liver was perfused with HEPES-buffered Hank's balanced salt solution. Hepatocytes were dispersed, washed, and purified on Percoll density gradient. The isolated hepatocytes were seeded in a rat tail collagen–coated 24-well cell culture plate at a density of 2.5×10^5 cells/ml.

Metabonomics Analysis of Mouse Liver Using GC-MS

The samples of mouse liver and GC-MS analysis were processed as reported previously (Cao et al., 2013). Briefly, ^{13}[C_2]-myristic acid (12.5 μg/ml) was used

as internal standard (IS). An ULTRA-TURRAX T25 homogenizer was used to homogenize 20 mg of liver tissue, and 30 μl of methoxyamine hydrochloride in pyridine (10 mg/ml) was added to the residue. After derivatizing for 16 hours, 30 μl of the *N*-methyl-n-trimethylsilane trifluoroacetamide reagent (1% Trimethylchlorosilane, v/v) was added. Finally, 30 μl of heptane solution containing external standard methyl myristate (30 μg/ml) was used as dissolving solvent. GC-MS analysis was performed using a Shimadzu GC-MS QP2010 Ultra gas chromatograph system coupled with mass spectrometer (Shimadzu Corporation, Kyoto, Japan). The MS data were acquired in full-scan mode with the *m/z* range of 50–700 at an acquisition rate of 5000 Hz. GC-MS solution software (Shimadzu Corporation) was used for the raw data acquisition and processing. Principal component analysis (PCA) and orthogonal partial least squares–discriminate analysis (OPLS-DA) were performed using SIMCA version 14.0.1 (Umetrics, Sweden) and MetaboAnalyst 4.0 (http://www.metaboanalyst.ca/). Statistical analyses were conducted by SPSS software version 19.0 (IBM Corp., Armonk). Heat maps and hierarchical cluster analyses were conducted using MeV 4.6.0 software.

Proteomics Analysis of Mouse Liver Using LTQ-Orbitrap XL MS

The samples of mouse liver and LTQ-Orbitrap XL MS analysis were processed as we described previously (Shao et al., 2017). Briefly, mouse liver (200 mg) was ground in liquid nitrogen, and 2 ml of Radio-Immunoprecipitation Assay lysate (containing 10 mM phenylmethylsulfonyl fluoride) was added to extract proteins. Then, 200 μg of protein was added in 10-kDa ultrafiltration tube, and then denaturation, alkylation, and trypsin digestion were carried out. The digestion reaction was terminated by 1 μl of trifluoroacetic acid. After centrifuging at 14,000*g* for 10 minutes, the effluent was collected and dried in a vacuum concentrator. The evaporated sample was redissolved with 50 μl of 0.1% formic acid aqueous solution and then desalted using zip-tip C18 tips. Online separation and determination of digested liver specimen were performed using an Ultimate 3000 RSLC nano system coupled to an LTQ-Orbitrap XL MS (Thermo Fisher Scientific, San Jose, CA). A sample equivalent to 10 μg protein was injected onto the reversed-phase trap column (Acclaim PepMap100 C18, 75 μm × 2 cm, 3 μm, 100 Å; Thermo Scientific). A series of nanoflow gradients were used to back-flush the trapped samples onto the nano-LC column (Acclaim PepMap RSLC, C18, 75 μm × 15 cm, 3 μm, 100 Å; Thermo Scientific) for chromatographic separation. The LTQ-Orbitrap XL MS was operated in a data-dependent mode to switch between MS^1 and Tandem mass spectrometry automatically. MS^1 survey scans (*m/z* 350–1800) were performed with a resolution of 60,000 at *m/z* 400. Electrospray voltage was 2.2 kV. Raw data were processed using Proteome Discoverer version 1.4 (Thermo Fisher Scientific, Waltham, MA). Protein identification was performed using Sequest HT engine combining the *Rattus norvegicus* database (Taxonomy 9606, http://www.uniprot.org/proteomes/).

Lipidomics Analysis of Mouse Liver Using Liquid Chromatography Quadrupole-Time-Of-Flight Mass Spectrometry

Mouse liver (50 mg) was homogenized in 200 μl of 75% methanol and 10 μl of the mixed internal standard solution (containing 40 μg/ml LPC 17:0, 200 μg/ml PC 14:0/14:0, 200 μg/ml LPE 14:0, 200 μg/ml PE 14:0/14:0, 400 μg/ml PS 14:0/14:0, 100 μg/ml TAG 17:0/17:0/17:0), followed by adding 500 μl of methyl tert-butyl ether. After vortex mixing for 1 hour, 125 μl of H_2O was added and settled for 5 minutes. The supernatant was dried and then redissolved in acetonitrile/isopropanol/water (60:35:5, v/v/v).

LC separation was performed using a Shimadzu UFLC-30A system (Shimadzu). All the components were eluted onto a Shimadzu Shim-pack VP-ODS column (5 μm, 150 × 2.0 mm Inside Diameter; Shimadzu). Mobile phase A was acetonitrile/water (60:40, v/v) containing 10 mmol/l of ammonium formate. MPB was acetonitrile/isopropanol (10:90, v/v) containing 10 mmol/l ammonium formate. A 30-minute gradient elution was as follows: 0–7 minutes, 30% MPB; 7–25 minutes, 30%–100% MPB; 25–30 minutes, 30% MPB. MS analysis was performed using an AB Sciex 5600+ Triple TOF MS system (Concord, Ontario, Canada), which operated in positive and negative ionization modes, respectively. The MS parameters were set as follows: gas 1, 50 psi; gas 2, 50 psi; curtain gas, 35 psi; MS^1 scan range 400–1000 (*m/z*); MS^2 scan range 100–1000 (*m/z*). In positive ionization mode, ion-spray voltage floating was 5.5 kV, and collision energy was 35 V. In negative ionization mode, ion-spray voltage floating was −4.5 kV, and collision energy was −35 V. All the LC and MS parameters were controlled by Analyst TF 1.7 software (Sciex, Concord). Peak recognition, extraction, and alignment were performed on MasterView 2.0 software (Sciex, Concord). MS^2 fragment ions of lipids were identified and confirmed by PeakView 1.2 software (Sciex, Concord) combining LipidBlast database. All the peaks were integrated by Multiquant 2.0 (Sciex, Concord).

Bioinformatics Analysis of Protein Data

The gene ontology function annotation of differential proteins was analyzed from three aspects of biologic process, molecular function, and cellular component by Blast GO to further understand the function of the 72 common differential proteins in the process of SLE's liver protection. Then, the Kyoto Encyclopedia of Genes and Genomes (KEGG) database was used to analyze the main biochemical metabolic pathways and signal transduction pathways involved in differentially expressed protein.

Determination of Aspartate Aminotransferase and Alanine Aminotransferase Activities in Serum

Serum AST and ALT activities were measured using commercial kits (Nanjing Jiancheng Institute of Biotechnology, Nanjing, China) by Reitman-Frankel colorimetric endpoint method. Absorbance was determined using a Synergy H1 microplate reader of multiwavelength measurement system (BioTek Instruments, Inc., Winooski, VT) at 510 nm.

Quantitative Reverse-Transcription Polymerase Chain Reaction Analysis

Total RNA was extracted from the liver samples using Trizol (Invitrogen Co., San Diego, CA). The RNA concentration and quality were determined using a Synergy H1 microplate reader of multiwavelength measurement system (BioTek Instruments, Inc.). cDNA was synthesized using a High-Capacity RNA-to-cDNA kit (Applied Biosystems, Foster City, CA). Quantitative reverse-transcription polymerase chain reaction was performed using the Thermal Cycler Dice Real Time System (Code: TP800; TaKaRa). The primer sets for the target genes are listed in Supplemental Table 2. Amplifications were performed starting with 1 minute at 95°C for template denaturation, followed by 40 cycles at 95°C for 15 seconds and 72°C for 0.5 minutes. The polymerase chain reaction amplifications were performed in a T3 Thermocycler (Biometra). The relative amounts of the RNAs were calculated using the comparative C_T method.

Western Blotting Analysis of Lipin1 and Lipin2

For Western blots, mouse liver was prepared as we previously described (Chen et al., 2020). Briefly, mouse liver was homogenized and diluted using 4× premixed protein sample buffer. The wells of a 6% acrylamide-bisacrylamide gel were loaded with 80 μg of protein. After being separated on a 10% SDS-polyacrylamide gel, the proteins were transferred onto a polyvinylidene difluoride membrane. Then, the proteins were subsequently transferred to a membrane (FFP24; Beyotime, China) blocked in 5% nonfat milk. After being washed for 30 minutes, the membrane was incubated in appropriate secondary antibodies. Bound immunoglobulins were visualized with the BeyoECL Star (Beyotime) on BIO-RAD ChemiDoc XRS^+. Grayscale analysis was carried out using Image J software (National Institutes of Health, open source).

Statistical Analysis

Student's *t* test or ANOVA were used to compare two groups and three or more groups, respectively. GraphPad Prism software (version 7.0) was used to calculate statistical significance. Statistically significant difference was considered for $P < 0.05$.

Results

Metabolomic Investigation of APAP-Induced Hepatotoxicity and Hepatoprotective Function of SLE. The hepatoprotective effect of SLE on APAP-induced liver injury was compared via analyzing the pathologic sections and determining the levels of ALT and AST in mouse liver samples of control, SLE, APAP, and SLE + APAP groups. As shown in the Supplemental Fig. 1, SLE has no significant effect on

the liver of healthy mice but can significantly alleviate the liver toxicity of APAP-induced liver injury mice.

The stability and repeatability of the GC-MS system for metabolomics analysis were validated by examining the retention time of the IS and the repeatability of pooled Quality Control samples. After GC-MS analysis of mouse liver samples of control, APAP, and SLE + APAP groups, a total of 64 compounds, including organic acids, sugars, purines, and amino acids, were identified by comparing the mass spectrum information of metabolites in National Institute of Standards and Technology and Wiley libraries. After normalizing the peak area of the identified metabolites with the IS, the pattern recognition technique, supervised OPLS-DA, was used to partition the data of control, APAP, and SLE + APAP groups. Sample distribution pattern in the score scatter plot indicated that there were significant differences in the metabolic profiling of mouse liver among the three groups (Fig. 1A). Compared with the control group, the metabolic profiling of the APAP group was shifted to the upper-right direction, and SLE dosing made the metabolic profiling move to the left quadrant, which suggested that SLE dosing had an obvious callback effect on APAP-induced liver metabolic profiling shift. The GC-MS spectra of the metabolites were analyzed based on mass spectra libraries, and the differential metabolites had to meet the criteria variable importance in the projection >1 and $P < 0.05$. A total of 35 kinds of differential small metabolites, mainly including maltose, adenylate, alanine, and glucose-6-phosphate, were screened from the liver samples. Besides, heat maps were created based on the average change fold of differential metabolites to intuitively evaluate their variation tendency among the control, APAP, and SLE + APAP groups. Obviously, the levels of glycine, maltose, adenylate, phenylalanine, glucose-6-phosphate, xylose, lactate, threonine, alanine, and proline in the liver of model mice were significantly lower than those of conventional mice. Administration of SLE could upregulate the intrahepatic concentrations of these metabolites (Fig. 1B). MetaboAnalyst software was used to enrich the pathway of these differential metabolites based on the Kyoto Encyclopedia of genes and genomes (KEGG) database, allowing us to identify enriched pathways from the differential expression profiling data and visualize changes in metabolite data by analyzing networks of genes and compounds. The results were shown in Fig. 1C and Supplemental Table 3. Urea cycle, ammonia recycling, arginine and proline metabolism, purine metabolism, glutamate metabolism, alanine metabolism, malate-aspartate shuttle, aspartate metabolism, gluconeogenesis, glucose-alanine cycle, nicotinate and nicotinamide metabolism, phenylalanine and tyrosine metabolism, glutathione metabolism, seleno amino acid metabolism, galactose metabolism, glycine and serine metabolism, phenylacetate metabolism, lactose degradation, glycolysis, cysteine metabolism, and starch and sucrose metabolism were found to play important roles in APAP-induced hepatotoxicity and hepatoprotective effect of SLE. The changes of urea cycle, ammonia recycling, and arginine and proline metabolism were the most significant among the control, APAP, and SLE + APAP groups. The disorder of urea cycle and ammonia synthesis recovery pathway can lead to the metabolism disorder of amino acids such as arginine, proline, and glutamine, which then leads to the disorder of lipid metabolism. Therefore, APAP-induced hepatotoxicity and the hepatoprotective effect of SLE may be closely related to lipid metabolism of liver.

Proteomic Investigation of APAP-Induced Hepatotoxicity and the Hepatoprotective Function of SLE. The whole protein of liver tissues of mice in control, APAP, and SLE + APAP groups was analyzed by LTQ-Orbitrap XL MS after a series of pretreatment processes such as denaturation, reduction, alkylation, enzymolysis, and desalting. A total of 7477 peptides and 1405 proteins were identified in mouse liver. All the identified proteins were quantitatively analyzed using MaxQuant (version 1.5.3) software based on the label-free method. PCA analysis was performed on the proteomic data of control, APAP, and SLE + APAP groups, and the results were shown in Fig. 2A. There was a significant difference in the proteome between the control group and APAP-induced liver injury groups. The regulation multiple >1.2 or <0.8 and P value <0.05 were used as the screening criteria to screen differential protein. A total of 133 differential proteins were identified between control and APAP groups, accounting for 9.4% of the total protein number. After APAP modeling, 78 differential proteins were significantly upregulated, and 55 differential proteins were significantly downregulated (Fig. 2B). We also screened the differential proteins in the livers of the APAP and the SLE + APAP groups. Compared with the APAP group, 162 differential proteins were found in the SLE + APAP group, accounting for 11.5% of the total protein number. After SLE treatment, 81 differential proteins were significantly upregulated, and 81 differential proteins were significantly downregulated (Fig. 2C). The overlapping relationship between the differential proteins of the control group and the APAP group and the differential proteins of the APAP group and the SLE + APAP group was shown in a Venn diagram, with a total of 72 protein overlaps (Fig. 2D). These results suggested that SLE might exert a hepatoprotective effect by regulating these 72 differential proteins.

As shown in Fig. 3A, the differential proteins were involved in 1757 biologic processes, 547 of which had a significant difference ($P < 0.05$). In addition, the differential proteins had 279 molecular functions, 116 of which had a significant difference ($P < 0.05$). The differentially expressed proteins were enriched into 57 signal pathways in KEGG database, 13 of which had a significant difference. Next, we enriched the biologic process function of the differential proteins. The results suggested that the main biologic functions of the differential proteins included cell attachment and location, cell composition or synthesis, cell development process, biologic regulation, immune process, metabolic process, response to stimulation, etc. (Fig. 3B). We mapped the protein-protein interaction of the differentially expressed proteins in the metabolic pathways. As shown in Fig. 3C, APAP-induced hepatotoxicity could significantly downregulate mug1, spa1b, serpin6b, pdia6, and CFL1, whereas SLE dosing could significantly reverse the downregulation of these proteolysis-related proteins. APAP-induced hepatotoxicity could also significantly downregulate glutathione transferases (Gstt3, Gstm1, Gstm2, Gstm3, and Gsta4) and platelet aggregation–related proteins (Fga, Fgb, and Fgg), whereas SLE dosing could significantly reverse the downregulation of these proteins. It should be noted that SLE could exert a hepatoprotective effect on APAP-induced hepatotoxicity by regulating the related proteins of lipid metabolism, including Cyp4a10, Cyp2b10, 3-oxo-5-beta-steriod 4-dehydrogenase, Hydroxyacyl-coenzyme A dehydrogenase, Retinal dehydrogenase, NADPH-cytochrome P450 reductase, Carboxylic ester hydrolase, Aldo-keto reductase family 1 member D1, and fatty acid–binding protein 1 (FABP1).

Lipidomic Investigation of APAP-Induced Hepatotoxicity and Hepatoprotective Function of SLE. The above results of metabonomics and proteomics both showed that the hepatoprotective effect of SLE was related to the lipid metabolism in mouse liver. Herein, lipidomics of mouse liver in control, APAP, and SLE + APAP groups were compared to identify the lipids related to the hepatoprotective effect of SLE. SCIEX 5600 Q-TOF MS was used to detect the lipids in mouse liver, and information-dependent acquisition was used under Electrospray Ionization positive and negative modes, respectively. A total of 211 kinds of lipids, including 57 TAGs, 43 PCs, 22 PEs, 22 kinds of DAGs, 16 phosphatidylinositols, 12 sphingomyelins, 12 PSs, eight LPCs, seven LPEs, six ceramides, and three lysophosphatidylinositols, were identified in mouse liver (Fig. 4A). In addition, there were

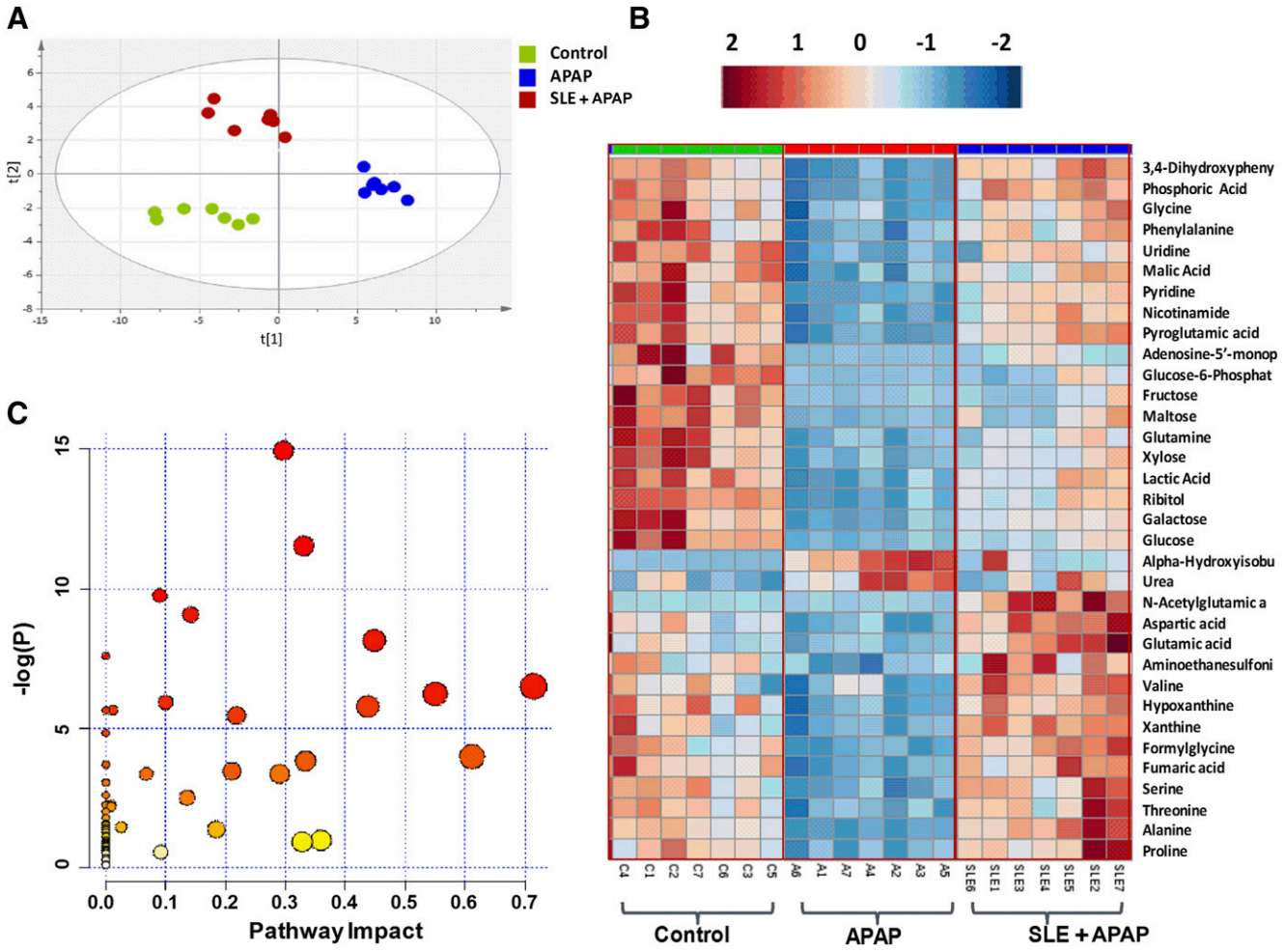

Fig. 1. Metabolomic investigation of APAP-induced hepatotoxicity and hepatoprotective function of SLE. (A) The score plots of the three groups and their OPLS-DA models for liver data (PC1, R2X = 0.657, R2Y = 0.438, Q2 = 0.424; PC2, R2X = 0.115, R2Y = 0.475, Q2 = 0.813; all five principal components). (B) Heatmap visualizing the intensities of differential metabolites in the liver samples (n = 7). (C) Pathway impact of metabolite pathways.

significant differences in the lipid profiling of mouse liver among the control, APAP, and SLE + APAP groups (Fig. 4B).

A total of 22 DAGs were identified in mouse liver, and DAG (16:0/18:2/0:0), DAG (18:1/18:1/0:0), and DAG (16:0/18:1/0:0) were much higher in content than other DAGs. In APAP-induced liver injury model mice, the content of 21 DAGs was significantly higher than that in normal mice, and SLE dosing could significantly reduce the content of these DAGs (Fig. 4C). The change folds of DAGs in control, APAP, and SLE + APAP groups were shown in Supplemental Table 4. A total of 57 TAGs were identified in mouse liver. In APAP-induced liver injury model mice, the content of 25 TAGs was significantly higher than that in control mice, and SLE dosing could significantly reduce the levels of six kinds of TAGs (Fig. 4D). The change folds of TAGs in control, APAP, and SLE + APAP groups were shown in Supplemental Table 5. In addition, the liver damage caused by APAP and SLE dosing was found to dramatically affect the levels of other lipids, such as LPC 16:0, LPC 18:0, LPC 18:1, LPC 18:2, LPC 20:0, LPC 20:1, LPC 20:4, LPC 22:6, PC (14:0/18:2), PC (14:0/16:1), PC (16:0/16:1), PE (16:1/18:3), etc.

Mechanism of APAP-Induced Hepatotoxicity and SLE on the Regulation of DAGs and TAGs. Lipins are phosphatidate phosphatase enzymes that catalyze the conversion of phosphatidic acids (PAs) to DAGs and thus act at a branch point for the synthesis of TAGs, zwitterionic phospholipids, or anionic phospholipids (Reue and Brindley, 2008). Herein, we measured the expressions of lipin1 and lipin2 in control, APAP, and SLE + APAP groups. In the APAP-induced liver injury model group, the expression of lipin1 was significantly upregulated, whereas SLE dosing could greatly reverse the upregulation of lipin1 (Fig. 5, A–C). In addition, SLE could also reverse the expression of lipin2 mRNA to a normal level, but neither APAP nor SLE had a significant effect on the expression of lipin2 protein (Fig. 5, D–F). CD36 is a single-chain transmembrane glycoprotein on the cell surface, which is involved in the metabolism and uptake of fatty acids. In the APAP-induced liver injury mice, the expression of CD36 was significantly lower than that in the control group, and SLE dosing could not reverse the downregulation of CD36 expression reduced by APAP (Fig. 5G). FABPs are the single most abundant proteins in the cytosol of cells, and they play important roles in the utilization of fatty acids in cells. Herein, expression of the liver-type fatty acid–binding protein (L-FABP) in mouse liver was measured. The results suggested that the expression of L-FABP in the APAP-induced model group was significantly lower than that in the control group, and SLE dosing could not reverse the downregulation of L-FABP expression reduced by APAP (Fig. 5H). Fatty acid transport proteins (FATPs) are multifunctional carrier proteins, which are involved in the synthesis of TAGs and promote the deposition of fat in the related tissues through the role of lipidization (Hatch et al., 2002). Therefore, FATPs are considered the most important factor involved in fatty acid transport and fat deposition. The effect of liver injury and SLE on the expression of FATP5, a FATP

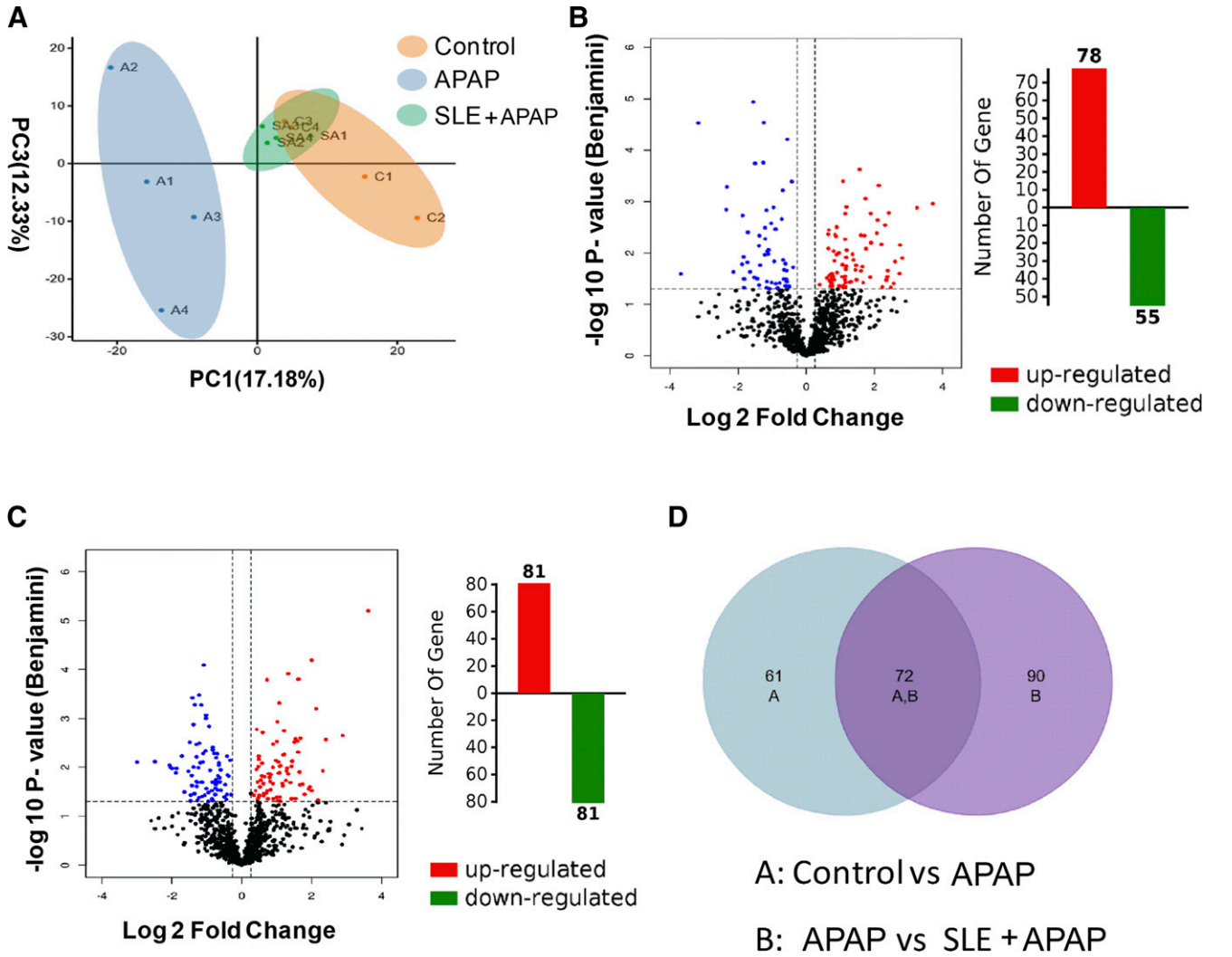

Fig. 2. Proteomics screening of differential proteins in control, APAP, and SLE + APAP mouse liver. (A) PCA analysis of control, APAP, and SLE + APAP mouse liver proteome. A, APAP-induced liver injury group; C, control group; SA, SLE + APAP group. (B) Volcano plot of differential abundance proteins and number of upregulated and downregulated proteins in control vs. APAP-treated mice. (C) Volcano plot of differential abundance proteins and number of upregulated and downregulated proteins in SLE + APAP vs. APAP-treated mice. (D) Venn diagram of differential abundance proteins identified in three experimental groups.

subtype distributed in the liver, was investigated in the present study. As shown in Fig. 5I, hepatotoxicity induced by APAP could lead to upregulation of FATP5 by about 50 times. After SLE administration, the level of FATP5 was significantly downregulated. Some of the fatty acids used in the synthesis of DAGs were derived from de novo synthesis, and the enzymes for the de novo synthesis of these fatty acids were acetyl CoA carboxylase 1 (ACC1) and fatty acid synthetase (FASN), respectively. Hepatotoxicity induced by APAP significantly reduced the expression of ACC1, whereas SLE dosing had no significant effect on the expression of ACC1 (Fig. 5J). SLE dosing could decrease the expression of FASN in mice with liver injury, although the effect of hepatotoxicity on the expression of FASN was not significant (Fig. 5K). In addition, diacylglycerol acyltransferase 2 (DGAT2) is a very important enzyme that can form TAGs by covalent bond of DAGs and acyl-CoA (Klaitong et al., 2017). Clearly, hepatotoxicity induced by APAP significantly enhanced the expression of DGAT2, and SLE dosing could reverse the upregulation of DGAT2 (Fig. 5L). Thus, the effect of APAP-induced hepatotoxicity and SLE dosing on the regulation of DAGs and TAGs was also closely related to lipin1, FATP5, and DGAT2.

Effect and Mechanism of DAGs on Liver Injury. Previous studies revealed that lipin activity could be inhibited by PNL (Grkovich et al., 2006; Albert et al., 2008; Brohee et al., 2015; Klaitong et al., 2017). Herein, we investigated the effect of PNL on DAGs and lipins in mouse liver. PNL was found to significantly reduce the content of DAGs in the liver of mice with APAP-induced hepatotoxicity but had no significant effect on the DAGs in the liver of control mice (Fig. 6, A and B). PNL could also significantly reduce the levels of serum ALT and AST in the mice with liver injury (Fig. 6, C and D). DAG (16:0/18:2/0:0) had a higher level than other DAGs in mouse liver and was used to investigate the influence of DAG on liver injury. As shown in Fig. 6E, DAG (16:0/18:2/0:0) could dose dependently reduce the survival rate of mouse primary hepatocytes. In addition, the inhibitor of DGAT2 (DGAT2i, PF-06424439) was used to further investigate the influence of DAG on liver injury. The results demonstrated that 20 μM of DGAT2i could dramatically decrease the survival rate of mouse primary hepatocytes (Fig. 6F), whereas PNL could dose dependently enhance the survival rate of hepatocytes (Fig. 6G).

DAGs are ligands of protein kinase C (PKC). The accumulation of DAGs in cells can activate PKC and then induce inflammation.

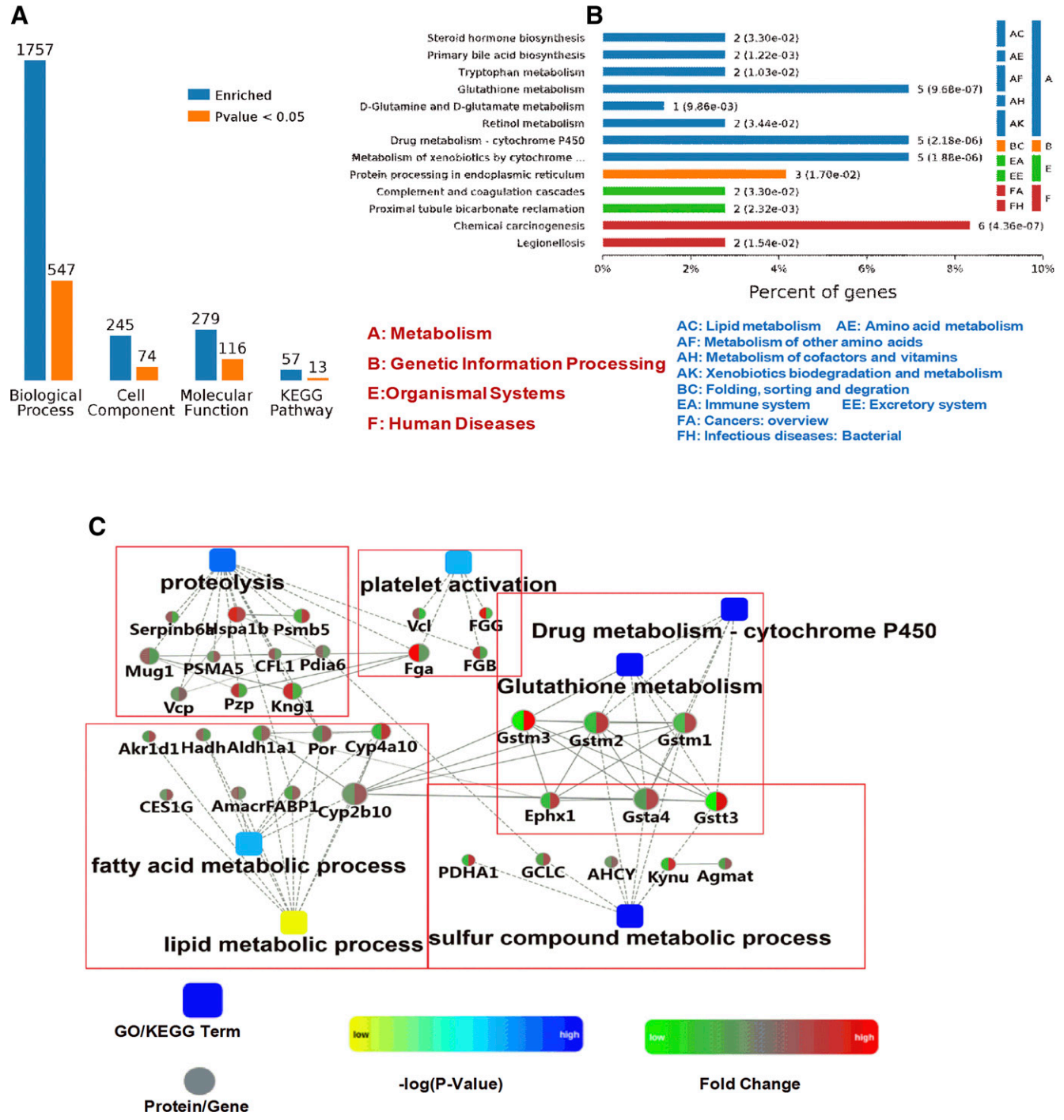

Fig. 3. Functional analysis of differential proteins in liver of control, APAP, and SLE + APAP mice. (A) Bioinformatics analysis of 72 identified differential proteins. (B) Class of enriched KEGG pathway. (C) Protein-protein interaction graph. Circle nodes refer to genes/proteins. The boxes refer to KEGG pathways or biologic processes with gradient colors from yellow (smaller *P* value) to blue (larger *P* value). Genes/proteins are colored in red (upregulation) and green (downregulation).

Therefore, the levels of PKCα, PKCβ, PKCγ, PKCδ, and PKCθ in control, APAP, and SLE + APAP groups were measured to clarify the mechanism of DAGs aggravating liver injury. There was no significant difference in PKCα expression among the three groups (Fig. 7A). The expression of PKCβ, PKCγ, PKCδ, and PKCθ in APAP-induced liver injury mice was significantly higher than that in the control group. After SLE administration, expressions of PKCβ, PKCγ, PKCδ, and PKCθ decreased to the normal level (Fig. 7, B–E). Among these PKCs, PKCγ was most affected by liver injury and SLE dosing. APAP-induced liver injury could upregulate PKCγ expression 15 times, and SLE dosing could make PKCγ expression return to the normal level.

Discussion

S. chinensis fructus, from the fruit of *S. chinensis* (Turcz.) Baill, has been widely used in TCM for the treatment of liver diseases in clinical settings for centuries (Cheng et al., 2013; Li et al., 2018). A large number

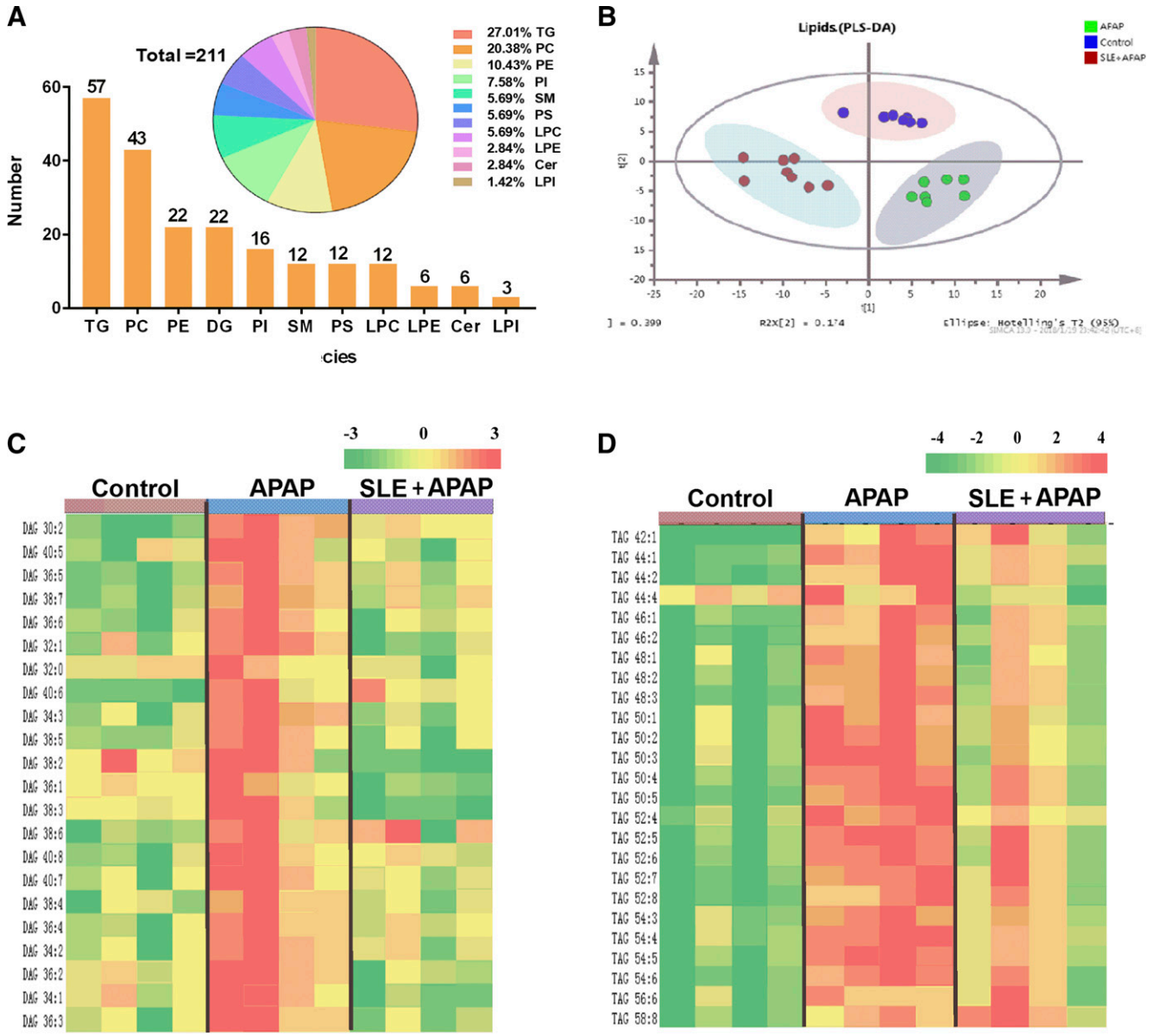

Fig. 4. Lipidomic investigation of APAP-induced hepatotoxicity and hepatoprotective function of SLE. (A) Counts of lipids identified and percentage of different lipid species. TG, DG, PI, SM, and Cer were defined as triacylglycerol, diglyceride, phosphatidylinositol, Sphngomyelin and Ceramide respectively. (B) PCA of lipidomics of control, APAP, and SLE + APAP mice. (C) Heatmap of DGs in control, APAP, and SLE + APAP mice. (D) Heatmap of TGs in control, APAP, and SLE + APAP mice.

of studies have proved that lignans are the main components of *S. chinensis* fructus (Liu et al., 2012; Chun et al., 2014; Zhang et al., 2018a). Just last year, we also demonstrated that SLE has a definite protective effect on APAP-induced liver injury on in vivo *and* in vitro models (Kang et al., 2019). To date, approximately 150 lignans have been identified from *S. chinensis* fructus. The chemical complexity, unknown targets, and unclear mechanism of SLE severely hamper its modernization and internationalization.

Although previous studies have yielded multifaceted mechanistic information about the hepatoprotective effect of SLE, the correlation among the metabolic events, progression of APAP-induced hepatotoxicity, and hepatoprotective effect of SLE have not been extensively examined. In this study, metabonomics approach was used to characterize the mechanism and target of SLE's liver protection. Sample distribution pattern in the score scatter plot indicated that APAP-induced hepatotoxicity caused a significant shift of small-molecule metabolic profiling, and SLE dosing had an obvious callback effect on APAP-induced liver metabolic profiling, which showed a novel correlation with the hepatoprotective effect of SLE on APAP-induced hepatotoxicity (Li et al., 2018; Kang et al., 2019). It should be noted that, compared with the control and SLE + APAP groups, urea cycle, ammonia recycling, arginine, and proline metabolism were altered in response to APAP-induced hepatotoxicity. Increasing evidence reveals that the disorder of urea cycle and ammonia synthesis recovery pathway can lead to the metabolism disorder of amino acids such as arginine, proline, and glutamine, which results in the metabolism disorder of lipids (Shimizu et al., 2015; Liu et al., 2019; Suzuki et al., 2019). Analyzed comprehensively, these results indicate that the APAP-induced hepatotoxicity and hepatoprotective effect of SLE might be attributable in part to the metabolism of lipids in liver. To further characterize the hepatoprotective effect of SLE, proteomics, another omics approach, was used to screen the target proteins in mouse liver

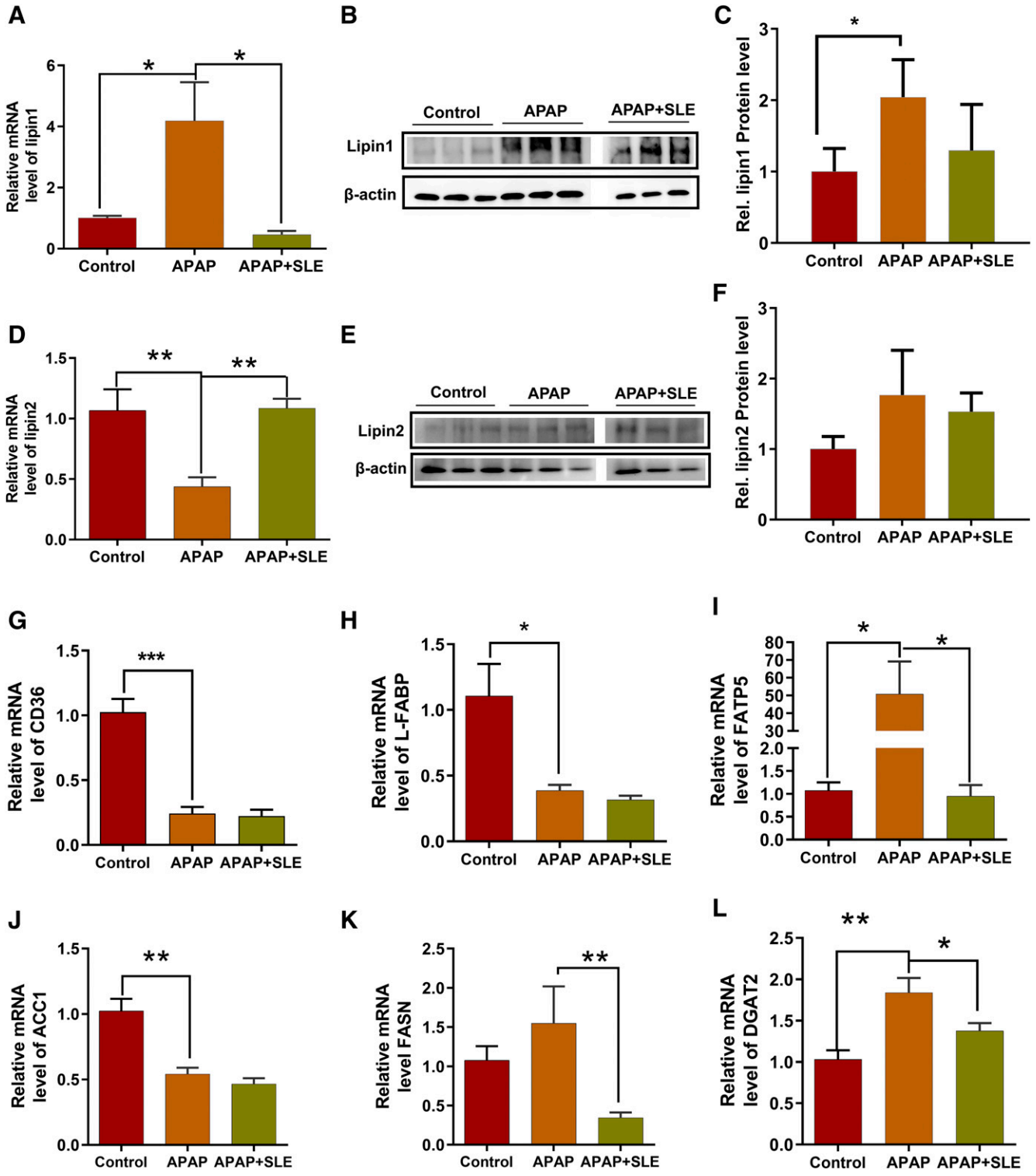

Fig. 5. Mechanism of APAP-induced hepatotoxicity and SLE on the regulation of DAGs and TAGs. (A) The relative mRNA level of lipin1 in the liver (n = 6). (B) Immunoblots for lipin1 (n = 3). (C) The protein levels of lipin1 (n = 3) in the liver. (D) The relative mRNA level of lipin2 in the liver (n = 6). (E) Immunoblots for lipin2 (n = 3). (F) The protein levels of lipin2 (n = 3) in the liver. The relative mRNA levels of (G) CD36, (H) L-FABP, (I) FATP5, (J) ACC1, (K) FASN, and (L) DGAT2 (n = 6). The results were shown with means ± S.D., and $^{*}P < 0.05$; $^{**}P < 0.01$; $^{***}P < 0.001$ were considered statistically significant.

from a holistic perspective. In recent years, comparative proteomics has become a robust approach for the demonstration of overall protein levels, and great progress has been made in the application of proteomics to determine the mechanism of the TCMs (Liu et al., 2016; Wen et al., 2018). In the present study, the proteomics approach reveals that proteolysis, platelet activation, drug metabolism, glutathione metabolism, lipid metabolic process, and the sulfur compound metabolic process play important roles in APAP-induced hepatotoxicity and the hepatoprotective effect of SLE. It is noteworthy that SLE could exert a hepatoprotective effect by

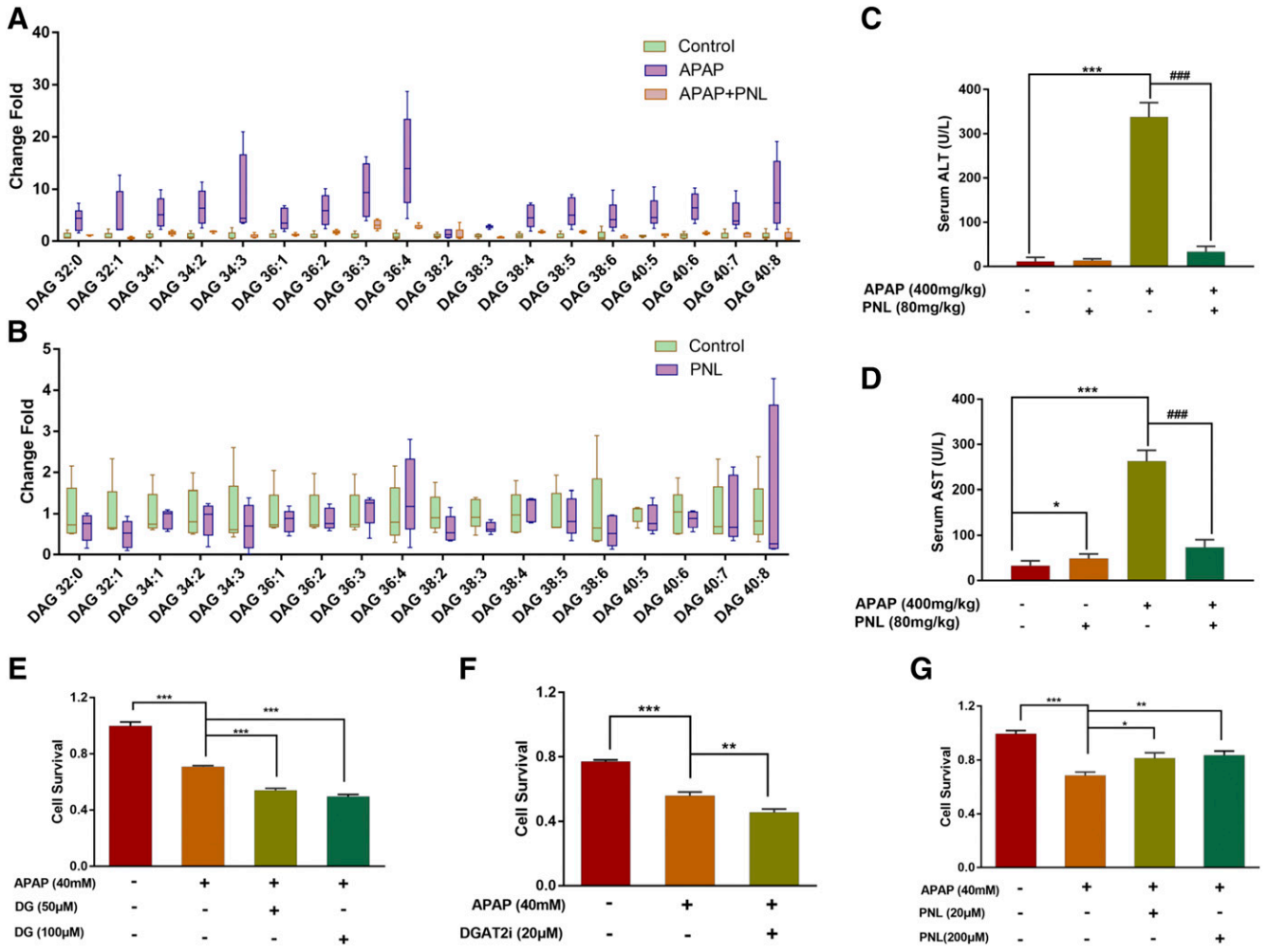

Fig. 6. Effect of DAGs on liver injury. (A) The influence of PNL on the fold change of DAGs in the liver of mice with APAP-induced hepatotoxicity ($n = 6$). (B) The influence of PNL on the fold change of DAGs in the liver of normal mice ($n = 6$). Serum levels of (C) ALT and (D) AST were measured using kits according to the manufacturer's instruction ($n = 6$). The influence of DAG (E), DGAT2i (F), and PNL (G) on the survival rate of mouse primary hepatocytes ($n = 6$). $^{*}P < 0.05$; $^{**}P < 0.01$; $^{***}P < 0.001$; $^{\#\#\#}P < 0.001$. DG was defined as diacylglycerol.

regulating the lipid metabolism–related proteins, including Cyp4a10, Cyp2b10, 3-oxo-5-beta-steriod 4-dehydrogenase, Hydroxyacyl-coenzyme A dehydrogenase, Retinal dehydrogenase, NADPH-cytochrome P450 reductase, Carboxylic ester hydrolase, Aldo-keto reductase family 1 member D1, and FABP1.

Metabonomics and proteomics approaches both show that APAP-induced hepatotoxicity and the hepatoprotective effect of SLE are associated with the regulation of lipid metabolism. Further evaluation of altered liver lipids in control, APAP, and SLE + APAP mouse is greatly needed to identify the lipids related to the hepatoprotective effect of SLE. The developments in lipidomics, including the combination of advanced analytical instrumentation and chemometric computation, provide another alternative technical platform for examining the lipid metabolic flux in a complex biomatrix (Shi et al., 2012; Hyötyläinen and Orešič, 2016). The indiscriminate and untargeted nature of lipidomic analysis can lead to the identification of novel biomarkers that guide subsequent investigations on the mechanism of diseases and chemically induced activities (Chen et al., 2008; Sreekumar et al., 2009). In this study, features of lipid alteration in mouse liver after treatment with APAP and SLE were identified, i.e., hepatic DAG and TAG levels significantly increased in APAP-induced liver injury mice, whereas these upregulated lipids could be reduced to a normal level by SLE dosing. In fact, the observation of DAG and TAG accumulation in this study is consistent with the reported blocked glucose metabolism, as the inhibition of β-oxidation of fatty acids is caused by APAP (Chen et al., 2009). Generally, the main sources of hepatic DAGs and TAGs include conversion from PAs, uptake and transport of free fatty acids, and de novo synthesis in liver.

In the process of transforming PAs into DAGs, phosphatidic acid phosphatases catalyze the formation of DAGs from PAs, which are the key enzymes to regulate the levels of PA and DAG in vivo (Eastmond et al., 2010). Lipins, as lipid phosphatidic acid phosphatases on endoplasmic reticulum, catalyze the dephosphorylation of phospholipid acid to form DAGs, and lipin activity acts at a branch point for the synthesis of triacylglycerol, zwitterionic phospholipids, or anionic phospholipids (Reue and Brindley, 2008). Previous studies suggest that lipin deficiencies are associated with the loss of normal glycerolipid synthetic capabilities as well as aberrant regulation of PA-mediated signaling cascades (Zhang and Reue, 2017). All three mammalian lipin proteins (lipin1, 2, and 3) have phosphatidic acid phosphatase enzyme activity, with specific activity for lipin1 somewhat higher than that for lipin2 and lipin3 (Donkor et al., 2007). In this study, APAP-induced hepatotoxicity was found to significantly upregulate lipin1, whereas the upregulated lipin1 could be reduced to a normal level by SLE dosing.

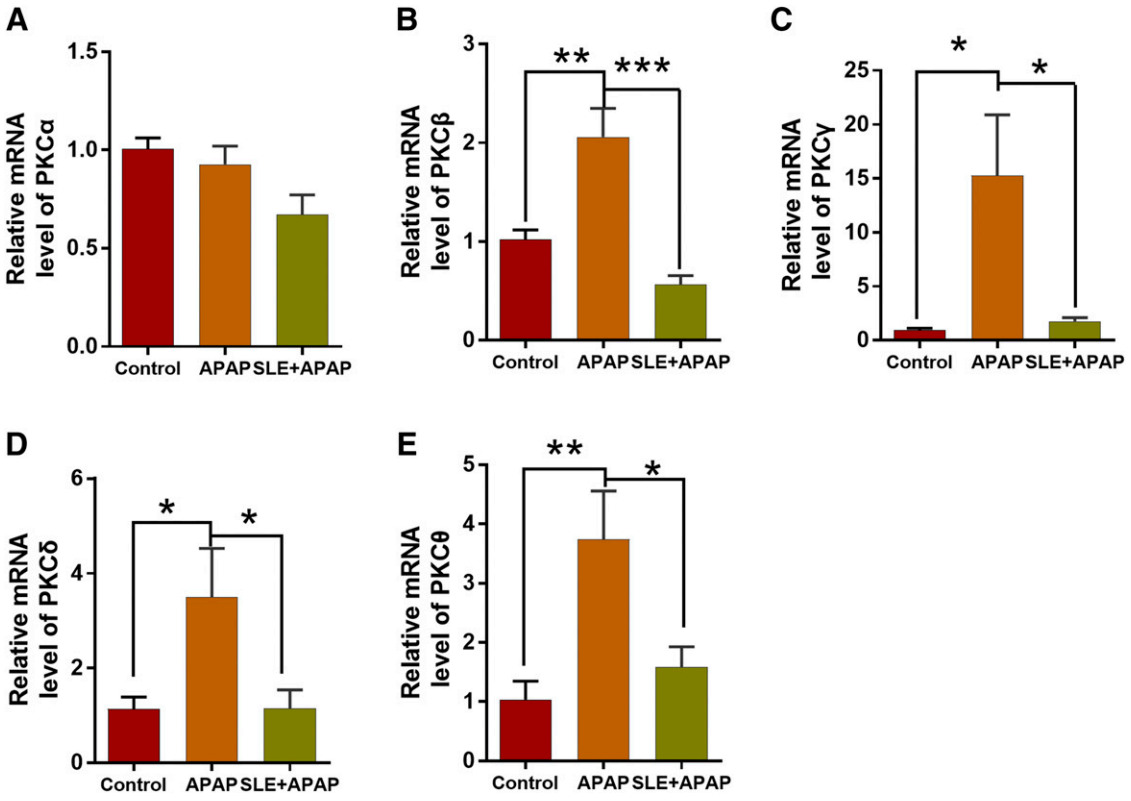

Fig. 7. The mechanism of DAGs aggravating liver injury. (A) The relative mRNA level of PKCα. (B) The relative mRNA level of PKCβ. (C) The relative mRNA level of PKCγ. (D) The relative mRNA level of PKCδ. (E) The relative mRNA level of PKCθ. *$P < 0.05$; **$P < 0.01$; ***$P < 0.001$.

Thus, lipin1 may be one of the targets of APAP-induced hepatotoxicity and the hepatoprotective effect of SLE. Uptake and intracellular trafficking of lipids are dependent on translocase (CD36), FABPs, and FATPs (Diaz et al., 2015). CD36 is a single-chain transmembrane glycoprotein on the cell surface that is involved in the uptake of long-chain fatty acids and contributes under excessive fat supply to lipid accumulation and metabolic dysfunction (Glatz and Luiken, 2017). In this study, altered CD36 expressions in control, APAP, and SLE + APAP mouse liver was evaluated, and the results suggest that APAP-induced hepatotoxicity significantly downregulates CD36 expression, and SLE dosing has no significant effect on CD36 expression. FABPs are a family of small and abundant proteins that are active in long-chain fatty acid uptake, transport, metabolism, oxidation, and storage (Xu et al., 2019a). Among these FABPs, L-FABP is highly expressed in both hepatocytes and enterocytes and plays a key role in high-fat diet–induced hepatic steatosis and diet-induced non-alcoholic steatohepatitis in vivo (Lin et al., 2018). Our results suggested that APAP-induced hepatotoxicity can significantly downregulate L-FABP expression, whereas the hepatoprotective effect of SLE does not depend on the regulation of L-FABP. FATPs are multifunctional carrier proteins, which can preferentially use the fatty acids transported to the cells for the synthesis of TAGs and promote the deposition of fat in the related tissues through the role of lipidization (Hatch et al., 2002). In general, FATPs are considered the most important factor involved in fatty acid transport and fat deposition. FATP5, an FATP subtype distributed in liver, was reported to be related to histologic progression and loss of hepatic fat in patients with nonalcoholic fatty liver disease (Enooku et al., 2020). Our research finds that hepatotoxicity induced by APAP can cause upregulation of FATP5 by about 50 times, and SLE administration can reduce FATP5 to a normal level. In addition, hepatotoxicity induced by APAP is found to significantly enhance the expression of DGAT2, an important enzyme for the formation of TAGs by covalent bond of DAGs and acyl-CoA. SLE administration could significantly reverse the upregulation of DGAT2. Therefore, the effect of APAP-induced liver injury and SLE on the regulation of DAGs and TAGs is also closely related to FATP5 and DGAT2.

The PKC family, lipid-activated kinases, always plays a significant role in the regulation of diverse cellular functions (Mamidi et al., 2014). DAGs act as endogenous ligands for the PKCs in the presence of anionic phospholipids, and the accumulation of DAGs in cells can activate PKC and then induce inflammation. Indeed, our study demonstrates that DAG (16:0/18:2/0:0) can dose dependently reduce the survival rate of mouse primary hepatocytes. PNL, an inhibitor of lipins, is found to significantly reduce the levels of serum ALT and AST in the mice with liver injury apart from dependently enhancing the survival rate of hepatocytes. To clarify the mechanism of DAGs aggravating liver injury, we measured the levels of PKCα, PKCβ, PKCγ, PKCδ, and PKCθ in control, APAP, and SLE + APAP mice. *S. chinensis* can significantly reverse the upregulation of PKCβ, PKCγ, PKCδ, and PKCθ induced by APAP.[1]C.Y., H.G., and Q.D. contributed equally to this work.

Acknowledgments

We acknowledge H.G., Y.S., D.K., T.Y., C.L., H.H., Y.D., and H.W. for contribution to study design and execution.

Authorship Contributions

Participated in research design: Yan, Guo, Ding, G. Wang, Liang.

Conducted experiments: Yan, Guo, Shao, Kang, Yu, Li, Huang, Du, H. Wang.

Contributed new reagents or analytic tools: Yan, Guo, Xie.

Performed data analysis: Yan, Liang.

Wrote or contributed to the writing of the manuscript: Yan, Ding, Guo, Hu, G. Wang, Liang.

References

Albert D, Pergola C, Koeberle A, Dodt G, Steinhilber D, and Werz O (2008) The role of diacylglyceride generation by phospholipase D and phosphatidic acid phosphatase in the activation of 5-lipoxygenase in polymorphonuclear leukocytes. *J Leukoc Biol* **83**:1019–1027.

Athuraliya TN and Jones AL (2009) Prolonged N-acetylcysteine therapy in late acetaminophen poisoning associated with acute liver failure--a need to be more cautious? *Crit Care* **13**:144.

Bernal W, Lee WM, Wendon J, Larsen FS, and Williams R (2015) Acute liver failure: a curable disease by 2024? *J Hepatol* **62** (Suppl):S112–S120.

Bhushan B and Apte U (2019) Liver regeneration after acetaminophen hepatotoxicity: mechanisms and therapeutic opportunities. *Am J Pathol* **189**:719–729.

Brohée L, Demine S, Willems J, Arnould T, Colige AC, and Deroanne CF (2015) Lipin-1 regulates cancer cell phenotype and is a potential target to potentiate rapamycin treatment. *Oncotarget* **6**: 11264–11280.

Cao B, Li M, Zha W, Zhao Q, Gu R, Liu L, Shi J, Zhou J, Zhou F, Wu X, et al. (2013) Metabolomic approach to evaluating adriamycin pharmacodynamics and resistance in breast cancer cells. *Metabolomics* **9**:960–973.

Chen C, Krausz KW, Shah YM, Idle JR, and Gonzalez FJ (2009) Serum metabolomics reveals irreversible inhibition of fatty acid beta-oxidation through the suppression of PPARalpha activation as a contributing mechanism of acetaminophen-induced hepatotoxicity. *Chem Res Toxicol* **22**:699–707.

Chen C, Shah YM, Morimura K, Krausz KW, Miyazaki M, Richardson TA, Morgan ET, Ntambi JM, Idle JR, and Gonzalez FJ (2008) Metabolomics reveals that hepatic stearoyl-CoA desaturase 1 downregulation exacerbates inflammation and acute colitis. *Cell Metab* **7**:135–147.

Chen H, Shen J, Li H, Zheng X, Kang D, Xu Y, Chen C, Guo H, Xie L, Wang G, et al. (2020) Ginsenoside Rb1 exerts neuroprotective effects through regulation of *Lactobacillus helveticus* abundance and $GABA_A$ receptor expression. *J Ginseng Res* **44**:86–95.

Chun JN, Cho M, So I, and Jeon JH (2014) The protective effects of Schisandra chinensis fruit extract and its lignans against cardiovascular disease: a review of the molecular mechanisms. *Fitoterapia* **97**:224–233.

Díaz P, Harris J, Rosario FJ, Powell TL, and Jansson T (2015) Increased placental fatty acid transporter 6 and binding protein 3 expression and fetal liver lipid accumulation in a mouse model of obesity in pregnancy. *Am J Physiol Regul Integr Comp Physiol* **309**: R1569–R1577.

Donkor J, Sariahmetoglu M, Dewald J, Brindley DN, and Reue K (2007) Three mammalian lipins act as phosphatidate phosphatases with distinct tissue expression patterns. *J Biol Chem* **282**: 3450–3457.

Eastmond PJ, Quettier AL, Kroon JT, Craddock C, Adams N, and Slabas AR (2010) Phosphatidic acid phosphohydrolase 1 and 2 regulate phospholipid synthesis at the endoplasmic reticulum in Arabidopsis. *Plant Cell* **22**:2796–2811.

Emwas AH, Luchinat C, Turano P, Tenori L, Roy R, Salek RM, Ryan D, Merzaban JS, Kaddurah-Daouk R, Zeri AC, et al. (2015) Standardizing the experimental conditions for using urine in NMR-based metabolomic studies with a particular focus on diagnostic studies: a review. *Metabolomics* **11**:872–894.

Enooku K, Tsutsumi T, Kondo M, Fujiwara N, Sasako T, Shibahara J, Kado A, Okushin K, Fujinaga H, Nakagomi R, et al. (2020) Hepatic FATP5 expression is associated with histological progression and loss of hepatic fat in NAFLD patients. *J Gastroenterol* **55**:227–243.

Glatz JF and Luiken JJ (2017) From fat to FAT (CD36/SR-B2): understanding the regulation of cellular fatty acid uptake. *Biochimie* **136**:21–26.

Grkovich A, Johnson CA, Buczynski MW, and Dennis EA (2006) Lipopolysaccharide-induced cyclooxygenase-2 expression in human U937 macrophages is phosphatidic acid phosphohydrolase-1-dependent. *J Biol Chem* **281**:32978–32987.

Hatch GM, Smith AJ, Xu FY, Hall AM, and Bernlohr DA (2002) FATP1 channels exogenous FA into 1,2,3-triacyl-sn-glycerol and downregulates sphingomyelin and cholesterol metabolism in growing 293 cells. *J Lipid Res* **43**:1380–1389.

Hyötyläinen T and Orešič M (2016) Bioanalytical techniques in nontargeted clinical lipidomics. *Bioanalysis* **8**:351–364.

Jiang Y, Fan X, Wang Y, Tan H, Chen P, Zeng H, Huang M, and Bi H (2015) Hepato-protective effects of six Schisandra lignans on acetaminophen-induced liver injury are partially associated with the inhibition of CYP-mediated bioactivation. *Chem Biol Interact* **231**:83–89.

Kang D, Shao Y, Zhu Z, Yin X, Shen B, Chen C, Xu Y, Shen J, Li H, Li X, et al. (2019) Systematically identifying the hepatoprotective ingredients of Schisandra lignan extract from pharmacokinetic and pharmacodynamic perspectives. *Phytomedicine* **53**:182–192.

Klaitong P, Fa-Aroonsawat S, and Chungjatupornchai W (2017) Accelerated triacylglycerol production and altered fatty acid composition in oleaginous microalga Neochloris oleoabundans by overexpression of diacylglycerol acyltransferase 2. *Microb Cell Fact* **16**:61.

Kuo YH, Li SY, Huang RL, Wu MD, Huang HC, and Lee KH (2001) Schizanrins [corrected] B, C, D, and E, four new lignans from Kadsura matsudai and their antihepatitis activities. *J Nat Prod* **64**:487–490.

Lan YL, Zhou JJ, Liu J, Huo XK, Wang YL, Liang JH, Zhao JC, Sun CP, Yu ZL, Fang LL, et al. (2018) Uncaria rhynchophylla ameliorates Parkinson's disease by inhibiting HSP90 expression: insights from quantitative proteomics. *Cell Physiol Biochem* **47**:1453–1464.

Li L, Zhang T, Zhou L, Zhou L, Xing G, Chen Y, and Xin Y (2014) Schisandrin B attenuates acetaminophen-induced hepatic injury through heat-shock protein 27 and 70 in mice. *J Gastroenterol Hepatol* **29**:640–647.

Li Y, Nie L, Jiang H, Lin J, Zhou H, Xie J, Qu Z, Qi D, and Zhang Y (2013) Metabonomics study of essential hypertension and its Chinese medicine subtypes by using gas chromatography-mass spectrometry and nuclear magnetic resonance spectroscopy. *Evid Based Complement Alternat Med* **2013**:625906.

Lin J, Zheng S, Attie AD, Keller MP, Bernlohr DA, Blaner WS, Newberry EP, Davidson NO, and Chen A (2018) Perilipin 5 and liver fatty acid binding protein function to restore quiescence in mouse hepatic stellate cells. *J Lipid Res* **59**:416–428.

Lin LL, Wang YH, Lai CY, Chau CL, Su GC, Yang CY, Lou SY, Chen SK, Hsu KH, Lai YL, et al. (2012) Systems biology of meridians, acupoints, and Chinese herbs in disease. *Evid Based Complement Alternat Med* **2012**:372670.

Liu C, Mao L, Ping Z, Jiang T, Wang C, Chen Z, Li Z, and Li J (2016) Serum protein KNG1, APOC3, and PON1 as potential biomarkers for yin-deficiency-heat syndrome. *Evid Based Complement Alternat Med* **2016**:5176731.

Liu H, Zhang J, Li X, Qi Y, Peng Y, Zhang B, and Xiao P (2012) Chemical analysis of twelve lignans in the fruit of Schisandra sphenanthera by HPLC-PAD-MS. *Phytomedicine* **19**: 1234–1241.

Liu MY, Tang D, Shi Y, Ma L, Li Y, Zhang Q, and Ruan J (2019) Short-term inhibition of glutamine synthetase leads to reprogramming of amino acid and lipid metabolism in roots and leaves of tea plant (Camellia sinensis L.). *BMC Plant Biol* **19**:425.

Liu X, Shi Y, Hu Y, Luo K, Guo Y, Meng W, Deng Y, and Dai R (2018) *Bupleurum marginatum* Wall.ex DC in liver fibrosis: pharmacological evaluation, differential proteomics, and network pharmacology. *Front Pharmacol* **9**:524.

Mamidi N, Panda S, Borah R, and Manna D (2014) Synthesis and protein kinase C (PKC)-C1 domain binding properties of diacyltetrol based anionic lipids. *Mol Biosyst* **10**:3002–3013.

Ohyama K, Baba M, Tamai M, Aibara N, Ichinose K, Kishikawa N, Kawakami A, and Kuroda N (2015) Proteomic profiling of antigens in circulating immune complexes associated with each of seven autoimmune diseases. *Clin Biochem* **48**:181–185.

Panossian A and Wikman G (2008) Pharmacology of Schisandra chinensis Bail.: an overview of Russian research and uses in medicine. *J Ethnopharmacol* **118**:183–212.

Reue K and Brindley DN (2008) Thematic Review Series: glycerolipids. Multiple roles for lipins/phosphatidate phosphatase enzymes in lipid metabolism. *J Lipid Res* **49**:2493–2503.

Selevsek N, Chang CY, Gillet LC, Navarro P, Bernhardt OM, Reiter L, Cheng LY, Vitek O, and Aebersold R (2015) Reproducible and consistent quantification of the Saccharomyces cerevisiae proteome by SWATH-mass spectrometry. *Mol Cell Proteomics* **14**:739–749.

Shao Y, Yin X, Kang D, Shen B, Zhu Z, Li X, Li H, Xie L, Wang G, and Liang Y (2017) An integrated strategy for the quantitative analysis of endogenous proteins: a case of gender-dependent expression of P450 enzymes in rat liver microsome. *Talanta* **170**:514–522.

Shi X, Yao D, Gosnell BA, and Chen C (2012) Lipidomic profiling reveals protective function of fatty acid oxidation in cocaine-induced hepatotoxicity. *J Lipid Res* **53**:2318–2330.

Shimizu N, Maruyama T, Yoshikawa N, Matsumiya R, Ma Y, Ito N, Tasaka Y, Kuribara-Souta A, Miyata K, Oike Y, et al. (2015) A muscle-liver-fat signalling axis is essential for central control of adaptive adipose remodelling. *Nat Commun* **6**:6693.

Sreekumar A, Poisson LM, Rajendiran TM, Khan AP, Cao Q, Yu J, Laxman B, Mehra R, Lonigro RJ, Li Y, et al. (2009) Metabolomic profiles delineate potential role for sarcosine in prostate cancer progression. *Nature* **457**:910–914.

Suzuki Y, Kido J, Matsumoto S, Shimizu K, and Nakamura K (2019) Associations among amino acid, lipid, and glucose metabolic profiles in childhood obesity. *BMC Pediatr* **19**:273.

Titz B, Gadaleta RM, Lo Sasso G, Elamin A, Ekroos K, Ivanov NV, Peitsch MC, and Hoeng J (2018) Proteomics and lipidomics in inflammatory bowel disease research: from mechanistic insights to biomarker identification. *Int J Mol Sci* **19**:2775.

Wen L, Liu YF, Jiang C, Zeng SQ, Su Y, Wu WJ, Liu XY, Wang J, Liu Y, Su C, et al. (2018) Comparative proteomic profiling and biomarker identification of traditional Chinese medicine-based HIV/AIDS syndromes. *Sci Rep* **8**:4187.

Xu H, Diolintzi A, and Storch J (2019a) Fatty acid-binding proteins: functional understanding and diagnostic implications. *Curr Opin Clin Nutr Metab Care* **22**:407–412.

Xu S, Chen Y, Ma Y, Liu T, Zhao M, Wang Z, and Zhao L (2019b) Lipidomic profiling reveals disruption of lipid metabolism in valproic acid-induced hepatotoxicity. *Front Pharmacol* **10**:819.

Yan R, Yang Y, and Chen Y (2018) Pharmacokinetics of Chinese medicines: strategies and perspectives. *Chin Med* **13**:24.

Yang L, Li M, Shan Y, Shen S, Bai Y, and Liu H (2016) Recent advances in lipidomics for disease research. *J Sep Sci* **39**:38–50.

Zhang M, Xu L, and Yang H (2018a) Schisandra *chinensis* fructus and its active ingredients as promising resources for the treatment of neurological diseases. *Int J Mol Sci* **19**:1970.

Zhang P and Reue K (2017) Lipin proteins and glycerolipid metabolism: roles at the ER membrane and beyond. *Biochim Biophys Acta Biomembr* **1859** (9 Pt B):1583–1595.

Zhang W, Huai Y, Miao Z, Qian A, and Wang Y (2019) Systems pharmacology for investigation of the mechanisms of action of traditional Chinese medicine in drug discovery. *Front Pharmacol* **10**:743.

Zhang Y, Lv X, Qu J, Zhang X, Zhang M, Gao H, Zhang Q, Liu R, Xu H, Li Q, et al. (2020) A systematic strategy for screening therapeutic constituents of Schisandra chinensis (Turcz .) Baill infiltrated blood-brain barrier oriented in lesions using ethanol and water extracts: a novel perspective for exploring chemical material basis of herb medicines. *Acta Pharm Sin B* **10**:557–568.

Zhang Y, Wang Y, Li S, Zhang X, Li W, Luo S, Sun Z, and Nie R (2018b) ITRAQ-based quantitative proteomic analysis of processed *Euphorbia lathyris* L. for reducing the intestinal toxicity. *Proteome Sci* **16**:8.

Address correspondence to: Yan Liang, Key Laboratory of Drug Metabolism & Pharmacokinetics, State Key Laboratory of Natural Medicines, China Pharmaceutical University, Tongjiaxiang 24, Nanjing 210009, China. E-mail: liangyan0679@163.com; or Guangji Wang, Key Laboratory of Drug Metabolism & Pharmacokinetics, State Key Laboratory of Natural Medicines, China Pharmaceutical University, Tongjiaxiang 24, Nanjing 210009, China. E-mail: guangjiwang@hotmail.com